Journal of
Synchrotron
Radiation

ISSN 0909-0495

Received 10 May 2010
Accepted 6 October 2010

Phase-contrast X-ray imaging of the gas diffusion layer of fuel cells

S. Takeya,[a]* A. Yoneyama,[b]* J. Miyamoto,[c]‡ Y. Gotoh,[a] K. Ueda,[b] K. Hyodo[d] and T. Takeda[e]

[a]Research Institute of Instrumentation Frontier, National Institute of Advanced Industrial Science and Technology (AIST), Central 5, 1-1-1 Higashi, Tsukuba 305-8565, Japan, [b]Advanced Research Laboratory, Hitachi Ltd, 2520 Akanuma, Hatoyama 350-0395, Japan, [c]Polymer Electrolyte Fuel Cell Cutting-Edge Research Center, National Institute of Advanced Industrial Science and Technology (AIST), 2-41-6 Aomi, Koto-ku, Tokyo 135-0064, Japan, [d]High Energy Accelerator Research Organization, 1-1 Oho, Tsukuba 305-0801, Japan, and [e]School of Allied Health Sciences, Kitasato University, 1-15-1 Kitasato, Minamiku, Sagamihara 252-0373, Japan.
E-mail: s.takeya@aist.go.jp, akio.yoneyama.bu@hitachi.com

The understanding of and *in situ* observation of the transport and distribution of water in carbon-paper gas diffusion layers (GDLs) using non-destructive imaging techniques is critical for achieving high performance in polymer electrolyte fuel cells (PEFCs). To investigate the behavior of water in GDLs of PEFCs, phase-contrast X-ray imaging *via* X-ray interferometric imaging (XII) and diffraction-enhanced imaging (DEI) were performed using 35 keV X-rays. The XII technique is useful for the radiographic imaging of GDLs and *in situ* observations of water evolution processes in operating PEFCs. DEI provides a way for tomographic imaging of GDLs in PEFCs. Because high-energy X-rays are applicable to the imaging of both carbon papers and heavy materials, which make up PEFCs, phase-contrast X-ray imaging techniques have proven to be valuable for investigation of GDLs.

Keywords: phase-contrast X-ray imaging; X-ray interferometer; fuel cell; gas diffusion layer; carbon paper.

1. Introduction

Polymer electrolyte fuel cells (PEFCs), which convert the chemical energy of hydrogen (H_2) directly into electrical energy, are considered to be one of the most promising energy-conversion devices (Steel & Heinzel, 2001; Bruijin, 2005). In PEFCs, water (H_2O) produced by the reaction of H_2 and oxygen (O_2) plays a crucial role, because PEFCs operate in a moderate temperature range between 333 and 383 K, which means the water can be in either a gas or liquid phase. If the catalyst layer and the adjacent porous gas diffusion layer (GDL) are filled with liquid water, the transport of reactant and product gases (O_2, H_2 and H_2O) is strongly hindered. This water blockage decreases the effective electrochemically active surface area of the cathode catalyst, which reduces the maximum achievable power density and the lifetime of the catalysts and the GDL. Therefore, understanding the transport and distribution of water in GDLs is critical to achieving high performance in PEFCs (Li *et al.*, 2008; Cindrella *et al.*, 2009).

Non-destructive imaging techniques, such as magnetic resonance imaging, neutron imaging, and X-ray absorption-contrast imaging, *e.g.* conventional X-ray computed tomography (X-ray CT) and synchrotron radiography, have been adapted to observe water accumulation and transport behavior in PEFCs (Bazylak, 2009). In the case of neutron imaging, the high water sensitivity of neutrons is useful for PEFC applications. In fact, several novel techniques demonstrating the in-plane neutron imaging of an operating PEFC were developed, but few groups worldwide are able to use this method owing to high costs and limited availability (St-Pierre, 2007; Mukundan & Borup, 2009). In the case of X-ray imaging, recent high special resolution measurements *via* the X-ray CT technique have successfully visualized each carbon fiber and pore structure within the GDL (Pfrang *et al.*, 2010; Ostadi *et al.*, 2010). An operating PEFC was also investigated through synchrotron X-ray radiography (Manke *et al.*, 2007, 2010; Mukaide *et al.*, 2008; Hartnig *et al.*, 2009). However, X-ray absorption-contrast imaging techniques can be applied for visualization of carbon paper and water in the absence of the other cell components, since lower X-ray photon energies (~10 keV) are sensitive to carbon paper and water but are readily absorbed by the other cell components. At high X-ray photon energies, phase shifts caused by materials comprised of low-atomic-number elements, such as inorganic materials composed of carbon, nitrogen, oxygen and hydrogen, are detectable but their absorption coefficients are almost zero. This is due to the fact that the X-ray-phase-shift cross section is more than 100 times larger than that of the X-ray absorption. The advantage of phase contrast is even more pronounced in the hard X-ray region. The ratios of the cross sections for carbon at 17.7 keV and 40 keV are about 100 and 500, respectively (Momose, 2005). Thus, phase-contrast X-ray imaging methods are viable for the imaging of carbon-paper GDLs in PEFCs.

‡ Present address: Tokyo University of Agriculture and Technology, Tokyo, Japan.

Several methods for detecting these phase shifts have been proposed: X-ray interferometry (Bonse & Hart, 1965; Momose *et al.*, 1995), diffractometry with perfect crystals (Goetz *et al.*, 1979; Davis *et al.*, 1995; Chapman *et al.*, 1997), a propagation-based Fresnel-pattern method (Snigirev *et al.*, 1995; Wilkins *et al.*, 1996) and interferometry with a Talbot grating (Momose *et al.*, 2003; Weitkamp *et al.*, 2005). Among these methods, X-ray interferometric imaging (XII) and diffraction-enhanced imaging (DEI) are the two major techniques for two- and three-dimensional observations of large samples, such as the biomedical imaging of mice. The density resolution of XII is higher than that of DEI (Yoneyama *et al.*, 2008). XII is also suitable for detecting gradual phase shifts and the absolute density of materials, but the observations are limited by a sample-outlining effect that occurs from the steep phase shifts caused by density difference between the sample and air. However, DEI offers a wide density dynamic range, which enables observation of samples containing regions with large density gradients (Yoneyama *et al.*, 2008).

In this study we applied XII and DEI techniques for the non-destructive imaging of carbon-paper GDLs at room temperature. Recently, a phase-contrast X-ray imaging method using a two-crystal X-ray interferometer was developed (Yoneyama *et al.*, 2005). A cryo-chamber that enables imaging from 193 K to room temperature was demonstrated in earlier experiments (Takeya *et al.*, 2006). This allows for the development of a method for *in situ* observation under various temperature conditions, such as the low-temperature imaging of super-cooled water or ice in PEFCs or high-temperature imaging.

2. Experimental

Experiments were performed using a 35 keV monochromatic synchrotron X-ray source at a vertical wiggler beamline (BL-14C) of the Photon Factory in Tsukuba, Japan. Monochromatic X-rays were selected using a Si(220) double-crystal monochromator, and the beam was enlarged horizontally by an asymmetric Si(220) crystal with 3.5° asymmetric angles.

For the XII measurements an X-ray interferometer was used to detect phase shifts by converting the phase shifts into interferograms. One of the two generated interference patterns was detected using a CCD-based X-ray imager (51 mm × 33 mm field of view, 4100 × 2650 pixels, and detector dimensions 12.5 µm × 12.5 µm), and the other pattern was detected using a feedback positioning system (Yoneyama *et al.*, 2004). This can be seen in Fig. 1(*a*). Three fringe scans with 3 s exposures were used to obtain a phase map, which is a spatial distribution of the phase shift. The field of view of the XII system was 25 mm × 35 mm with a spatial resolution of 40 µm.

For the DEI measurements the incident monochromatic X-ray beam enlarged horizontally by the asymmetric Si(220) crystal irradiates the sample. The X-ray beam that passes through the sample was diffracted by a Si(220) analyzer crystal and entered the X-ray imager. This can be seen in Fig. 1(*b*). The phase map was produced using 21 images obtained by scanning the analyzer crystal with a 3 s exposure time at each position. The field of view of the DEI system was 25 mm × 35 mm with a spatial resolution of 40 µm. To obtain three-dimensional phase-contrast computed tomography images, the carbon paper was rotated 180° in 0.72° steps. For more details on phase-contrast X-ray imaging systems, refer to Yoneyama *et al.* (2008).

In this study, three different GDLs made of PAN carbon fiber, TGP-H-090 (Toray Industrial), SIGRACET® 24AA and 24BA (SGL GROUP), were measured for comparison. For the GDL measurements the carbon-paper sample was set perpendicular to the X-ray beam path.

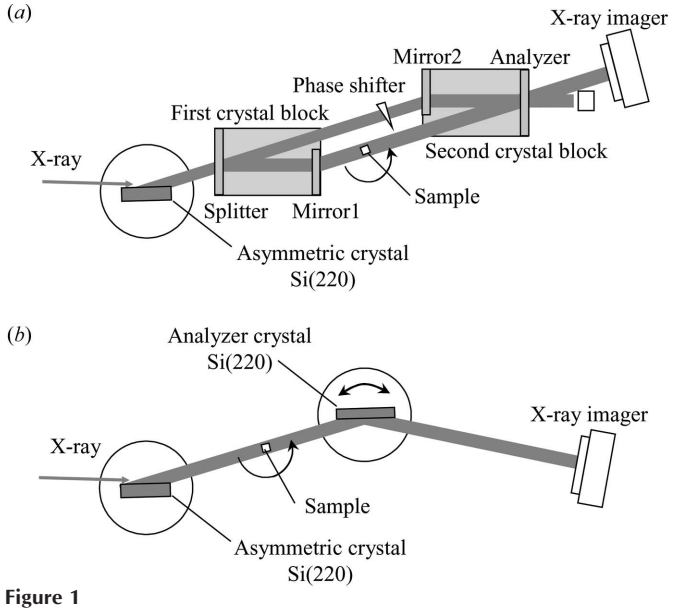

Figure 1
Schematic of the experimental phase-contrast X-ray imaging set-up. Top view of the XII (*a*) and DEI (*b*) methods. Here, incident X-rays in both experiments were enlarged horizontally by an asymmetric Si(220) crystal.

3. Results and discussion

Fig. 2 shows radiographic images of the three different carbon-paper types. In the XII images of 200 µm-thick 24AA and 24BA the details of individual carbon fibers are visualized in spite of the pronounced density difference between the sample and air. However, 280 µm-thick T90 carbon paper is sterically crowded owing to its large

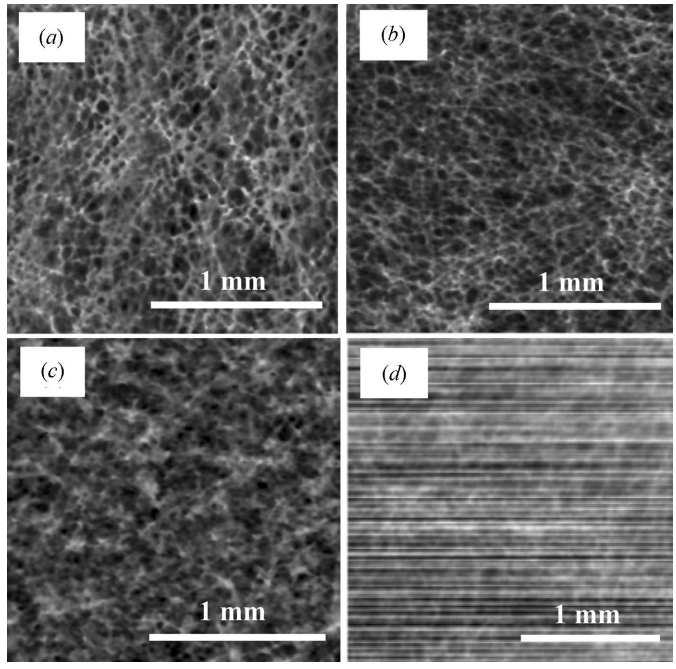

Figure 2
Radiographic images of PAN carbon-fiber GDLs. (*a*) 24AA, (*b*) 24BA and (*c*) T90 carbon-paper images obtained by using XII. A radiographic image obtained *via* DEI of 24BA carbon paper is also shown for comparison (*d*).

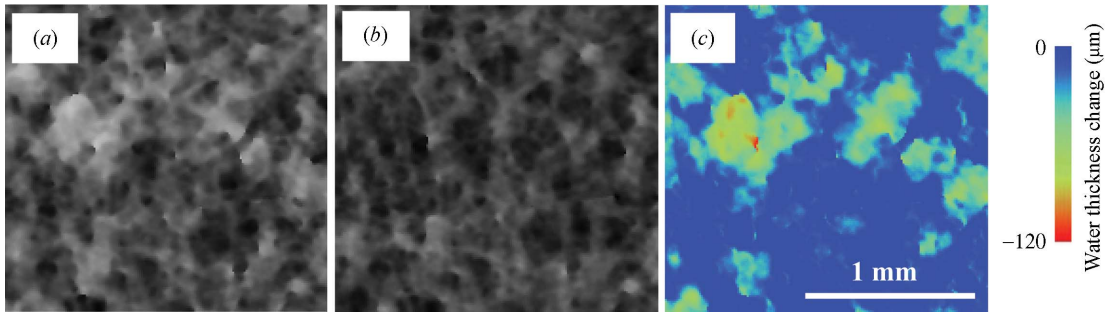

Figure 3
Radiographic images of water-sprayed T90 carbon paper obtained by using XII. Images obtained (*a*) following the water spray and (*b*) after drying. The change of water distribution is shown in the residue image (*c*). After some time, the water evaporates and the pores dry in the 280 μm-thick carbon paper.

thickness. The DEI image of 24BA carbon paper visualizes carbon fibers, but the image has high horizontal noise, which is due to the integral calculation used to obtain the phase map (Yoneyama *et al.*, 2008).

Fig. 3 shows radiographic images of carbon paper measured by XII just after being sprayed with water and after drying. Here, the water distribution of the T90 carbon paper is visualized. The residue image also shows the change in water distribution despite the fact that the radiographic image is sterically crowded owing to the thickness of the sample. An analysis of the residue image shows the change in water distribution quantitatively. It should also be noted that each radiographic image was measured for only 3 s. Therefore, this technique is viable for *in situ* observations of the water evolution process within operating PEFCs.

Fig. 4 shows a three-dimensional rendering of the DEI cross-sectional image of the carbon papers. The tomographic scan was only successfully performed using conventional reconstruction algorithms over an angular window, ±85°, owing to the large density difference between the carbon papers and air. However, the carbon papers were successfully imaged using conventional reconstruction algorithms. It is also shown that the interior of the thin carbon paper was visualized artifact-free in the cross-sectional image. This can be seen in the radiographic images shown in Figs. 2(*a*) and 2(*c*). For the XII measurements the tomographic scan was only successfully performed over less than ±45°, and a visualization of these carbon papers was not possible to obtain using conventional reconstruction algorithms. Since the density dynamic range is wide, the DEI technique allows us to visualize each carbon fiber within the carbon paper. Therefore, our results suggest that the XII method is useful for radiographic imaging, and the DEI method allows for the tomographic imaging of carbon-paper GDLs using 35 keV X-rays.

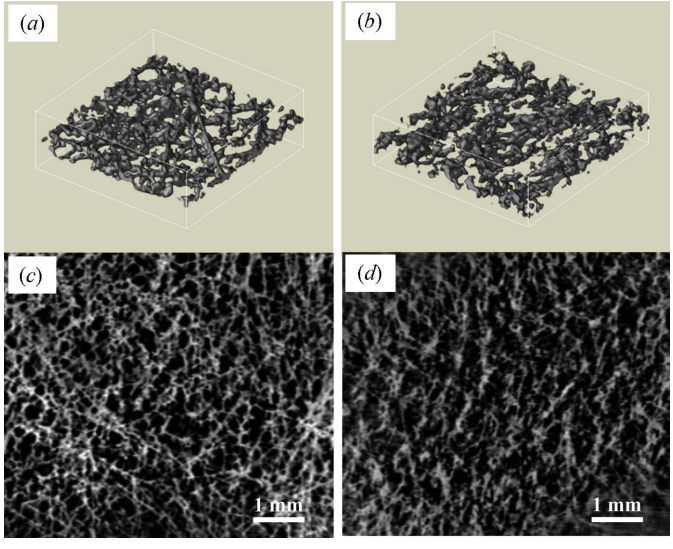

Figure 4
Three-dimensional cut-out image of (*a*) 24AA and (*b*) T90 carbon papers obtained *via* DEI. Here, an area of dimension 2.5 mm × 2.5 mm is extracted. Cross-sectional images of (*c*) 24AA and (*d*) T90 carbon papers, which were obtained from the three-dimensional data set, are also shown for comparison.

For comparison, the X-ray absorption-contrast imaging technique was also used on GDLs using 35 keV monochromatic synchrotron X-rays. However, the GDLs could not be visualized owing to the very high X-ray transmissivity of carbon at 35 keV, which is 99% for a 200 μm carbon layer. At the lower X-ray energies the transmissivity of carbon is relatively low; for example, the transmissivity at 8 keV and 17.5 keV is 82% and 98%, respectively. Therefore, lower-energy X-rays are useful in the X-ray absorption-contrast technique. However, the transmissivities of heavier materials is small for lower X-ray photon energy. In fact, the transmissivities of a 10 μm platinum (Pt) layer at 8 keV, 17.5 keV and 35 keV are 1%, 10% and 69%, respectively. This suggests that lower X-ray photon energies are not acceptable for imaging carbon paper adjacent to a Pt layer, which is the case for PEFC GDLs. However, we showed that phase-contrast X-ray imaging using a 35 keV X-ray source is useful for the imaging of both carbon paper and heavy materials. Therefore, we conclude that phase-contrast X-ray imaging at 35 keV is a suitable technique for PEFC imaging.

Recently, the imaging of a small PEFC, which had an active area of approximately 0.07 cm^2, using the phase-contrast Fresnel-pattern-based X-ray imaging method was performed during operation of the device (Schneider *et al.*, 2010). In this case the contrast outlining of surfaces and structural boundaries, where the refractive index changes abruptly, can be visualized with high-spatial resolution without the need for additional optics (Momose, 2005). However, the XII and DEI techniques are useful for relatively large size samples (∼10 cm^2), which we have shown in this study. In addition, the XII and DEI techniques are sensitive to slowly varying structures with high density resolution (Pagot *et al.*, 2005; Yoneyama *et al.*, 2008). Each technique using phase-contrast X-ray imaging has its advantages and disadvantages. Therefore, combined, these methods may provide the means to gather valuable insight into the behavior of liquid water accumulation and transport within GDLs.

4. Summary

Carbon-paper GDLs were imaged *via* phase-contrast X-ray imaging by means of XII and DEI techniques. For a comparison of these methods, three different carbon-paper samples were imaged at room

temperature using 35 keV X-rays. The XII method is useful for the radiographic imaging of GDLs and *in situ* observations of the water evolution process in operating PEFCs. The DEI method is not suitable for the radiographic imaging of GDLs because of its high horizontal noise. However, the DEI method provides a way for the tomographic imaging of GDLs in PEFCs.

Since phase-contrast X-ray imaging with 35 keV X-rays is applicable to the imaging of heavy materials together with carbon paper, these phase-contrast X-ray imaging techniques have proven to be valuable for the investigation of GDLs. While further experiments are required for the understanding of all phenomena in GDLs, we have shown that these phase-contrast X-ray imaging techniques enable the *in situ* observation of water accumulation and transport processes in GDLs.

This study was carried out under Proposal Nos. 2009S2-006 and 2008G120, and was approved by the High Energy Accelerator Research Organization.

References

Bazylak, A. (2009). *Int. J. Hydrogen Energy*, **34**, 3845–3857.
Bonse, U. & Hart, M. (1965). *Appl. Phys. Lett.* **6**, 155–156.
Bruijin, F. (2005). *Green Chem.* **7**, 132–150.
Chapman, D., Thomlinson, W., Johnston, R. E., Washburn, D., Pisano, E., Gmur, N., Zhong, Z., Menk, R., Arfelli, F. & Sayers, D. (1997). *Phys. Med. Biol.* **42**, 2015–2025.
Cindrella, L., Kannan, A. M., Lin, J. F., Saminathan, K., Ho, Y., Lin, C. W. & Wertz, J. (2009). *J. Power Sources*, **194**, 146–160.
Davis, T. J., Gao, D., Gureyev, T. E., Stevenson, A. W. & Wilkins, S. W. (1995). *Nature (London)*, **373**, 595–598.
Goetz, K., Kalashnikov, M. P., Mikhailov, Yu. A., Sklizkov, G. V., Fedotov, S. I., Foerster, E. & Zaumseil, P. (1979). *Sov. J. Quantum Electron.* **9**, 607–610.
Hartnig, C., Manke, I., Kuhn, R., Kleinau, S., Goebbels, J. & Banhart, J. (2009). *J. Power Sources*, **188**, 468–474.
Li, H., Tang, Y., Wang, Z., Shi, Z., Wu, S., Songa, D., Zhang, J., Fatih, K., Zhang, J., Wang, H., Liu, Z., Abouatallah, R. & Mazza, A. (2008). *J. Power Sources*, **178**, 103–117.
Manke, I., Hartnig, C., Grünerbel, M., Lehnert, W., Kardjilov, N., Haibel, A., Hilger, A., Banhart, J. & Riesemeier, H. (2007). *Appl. Phys. Lett.* **90**, 174105.
Manke, I., Hartnig, C., Kardjilov, N., Riesemeier, H., Goebbels, J., Kuhn, R., Kuger, P. & Banhart, J. (2010). *Fuel Cells*, **10**, 26–34.
Momose, A. (2005). *Jpn. J. Appl. Phys.* **44**, 6355–6367.
Momose, A., Kawamoto, S., Koyama, I., Hamaishi, Y., Takai, K. & Suzuki, Y. (2003). *Jpn. J. Appl. Phys.* **42**, L866–L868.
Momose, A., Takeda, T. & Itai, Y. (1995). *Rev. Sci. Instrum.* **66**, 1434–1436.
Mukaide, T., Mogi, S., Yamamoto, J., Morita, A., Koji, S., Takada, K., Uesugi, K., Kajiwara, K. & Noma, T. (2008). *J. Synchrotron Rad.* **15**, 329–334.
Mukundan, R. & Borup, R. L. (2009). *Fuel Cells*, **9**, 499–505.
Ostadi, H., Rama, P., Liu, Y., Chen, R, Zhang, X. & Jiang, K. (2010). *Microelectron. Eng.* **87**, 1640–1642.
Pagot, E., Fiedler, S., Cloetens, P., Bravin, A., Coan, P., Fezzaa, K., Baruchel, J. & Hartwing, J. (2005). *Phys. Med. Biol.* **50**, 709–724.
Pfrang, A., Veyret, D., Sieker, F. & Tsotridis, G. (2010). *Int. J. Hydrogen Energy*, **35**, 3751–3757.
Schneider, A., Wieser, C., Roth, J. & Helfen, L. (2010). *J. Power Sources*, **195**, 6349–6355.
Snigirev, A., Snigireva, I., Kohn, V., Kuznetsov, S. & Schelokov, I. (1995). *Rev. Sci. Instrum.* **66**, 5486–5492.
Steel, B. C. H. & Heinzel, A. (2001). *Nature (London)*, **414**, 345–352.
St-Pierre, J. (2007). *J. Electrochem. Soc.* **154**, B724–B731.
Takeya, S., Honda, K., Yoneyama, A., Hirai, Y., Okuyama, J., Hondoh, T., Hyodo, K. & Takeda, T. (2006). *Rev. Sci. Instrum.* **77**, 053705.
Weitkamp, T., Diaz, A. & David, C. (2005). *Opt. Express*, **13**, 6296–6304.
Wilkins, S. W., Gureyev, T. E., Gao, D., Pogany, A. & Stevenson, A. W. (1996). *Nature (London)*, **384**, 335–338.
Yoneyama, A., Jin, W., Hyodo, K. & Takeda, T. (2008). *Med. Phys.* **35**, 4724–4734.
Yoneyama, A., Takeda, T., Tsuchiya, Y., Wu, J., Lwin, T. T. & Hyodo, K. (2004). *AIP Conf. Proc.* **705**, 1299.
Yoneyama, A., Takeda, T., Tsuchiya, Y., Wu, J., Lwin, T.-T., Hyodo, K. & Hirai, Y. (2005). *J. Synchrotron Rad.* **12**, 534–536.